2011 IEEE/RSJ International Conference on
Intelligent Robots and Systems
September 25-30, 2011. San Francisco, CA, USA

Robot for Ultrasound-Guided Prostate Imaging and Intervention

Chunwoo Kim, Felix Schäfer, Doyoung Chang, Doru Petrisor, Misop Han, Dan Stoianovici

Abstract — **The paper presents a new robot for manipulating a transrectal ultrasound probe for image-guided intervention of the prostate, the TRUS robot. The robot positions and orients the probe for image scanning and needle targeting of the prostate. Image slices and their respective position are mapped three-dimensionally to render volumetric images.**

The robot is designed to accommodate the constraints of the clinical prostate intervention. The robot includes all 4 degrees-of-freedom that are available in manual handling of the probe. In-vitro studies on pelvic mockups verify 3D imaging capabilities. The robot is clinically used in robot-assisted laparoscopic radical prostatectomy for providing intraoperative ultrasound-based navigation for the surgeon.

I. Introduction

The recent trend towards minimally invasive therapy in medicine poses new challenges to surgeons due to reduced access and visualization. Medical imaging such ultrasound, computed tomography (CT), or magnetic resonance imaging (MRI) are used to augment direct visualization methods. New robotic technologies are then used to guide the intervention based on these images.

Due to their accuracy and controlled motion capabilities, robots have been used in image-guided interventions (IGI) for precisely positioning needles or other instruments for biopsy and delivering therapy [1-8]. Several MRI and CT guided robots have been reported [1, 4, 6-7] to facilitate access within the scanner, reduce radiation exposure, and guide the instrument in the image space.

For ultrasound, however, a robot may also serve an imaging role by providing the scanning motion for 3-D imaging. Typical ultrasound equipment provides 2-D images requiring mnemonic interpretation by the physician. The robot not only moves the probe to sweep the region of interest but also tracks its location to tag each image slice with its position data for 3-D reconstruction. As such, an ultrasound robot manipulator may serve as an ultrasound scanner.

3-D ultrasound is not new. First, 3-D probes use scanning motion internal to the probe or arrays of sensors to create the image. These machines are typically expensive and provide lower 2-D image quality than traditional probes. With 2-D probes, 3-D imaging has been created by tracking the location of the probe in freehand motion by either optical, electromagnetic, or with encoded arms. These are commonly termed as 3-D freehand ultrasound [9], and have been used in IGI tests and applications [3, 5, 8]. On the other hand, in addition to tracking, robots also provide controlled motion and probe locking, which render additional advantages relative to freehandling. For example, locking can hold the probe on target while a physician inserts the needle and takes a biopsy. Controlled motion gives more uniform scanning in a specified direction and with uniformly distributed slices. Other potential advantages include precise revisiting of a specific anatomical site, steady monitoring of an organ motion and deformations. The robot also replaces the tracker, obliterating line-of-sight problems common with optical tracking and stray noise associated with electromagnetic instruments.

Several robotic devices have been proposed for manipulating abdominal [10] and transrectal ultrasound (TRUS) [2, 11] probes. For needle interventions, these systems typically handle the needle (or even multiple needles [11]) but offer limited means of probe manipulation, such as longitudinal probe motion for transversal imaging of the gland.

In this paper we present a new TRUS probe manipulator, named Euler-2, designed for image-guided prostate interventions. The robot is built under the clinical constraints of the transrectal prostate intervention. The paper describes the structure, design, and kinematics of the robot, validates scanning capabilities, and presents its initial clinical application.

II. Manipulator design

The design of the robot is tailored to the constraints of the prostate intervention: The probe is manipulated similar to usual TRUS freehand motion; Manipulation minimizes lateral displacements at the entry point; The robot manipulates the probe to view the entire prostate; The size of the robot is compact to reduce interference with the patient and other medical devices; For safety, the robot should also minimize the amount of interference with the body, and minimize prostate deformations for consistent imaging.

As such, the TRUS robot was built with four degrees of freedom (DOF) as shown in Figure 1. According to their functional role, two rotary DOF pivot the probe about a fulcrum (RCM0 & RCM1) to accommodate anatomical constraints at the entry point, and two DOF rotate and translate the probe (TRUS-R & TRUS-T). These are implemented by a Remote Center of Motion (RCM) module and TRUS driver respectively.

Manuscript received March 14, 2011. This work was supported in part by Award CA141835 from the National Cancer Institute, the Prostate Cancer Research Program Training Award of the Department of Defense, Hitachi Medical America and the Sidney Kimmel Comprehensive Cancer Center at Johns Hopkins.

All authors are with Urology Robotics Laboratory, Johns Hopkins University, Baltimore, Maryland, USA. (e-mail: dss@jhu.edu)

The RCM is a ubiquitous mechanism for minimally invasive robots to provide key-hole access through a port or natural orifice [12]. Our RCM mechanism is a compact implementation of the mechanism using belts.

The TRUS driver attaches to the RCM module and supports the TRUS probe. The design of the TRUS driver presents a horseshoe construction (Figure 1) thus clearing the space above the probe for passing needles through the needle-guide of the probe. A passive arm supports the assembly with respect to a procedure table. The joints of the passive arm can be released and locked for initial placement of the probe as needed for the intervention.

Furthermore, in order to reduce prostate deformations and interference with the body, the robot is also equipped with force sensors to monitor forces and moments acting on the probe.

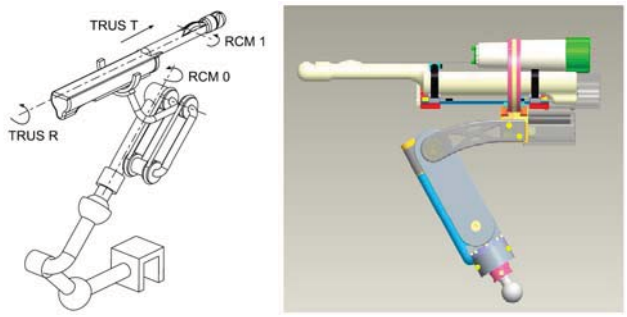

Figure 1: Schematic of the TRUS Robot

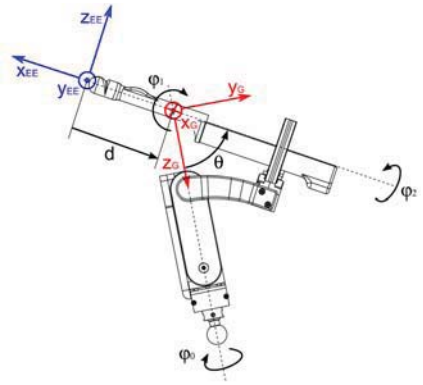

Figure 2: Coordinate system of the TRUS Robot

A. Forward Kinematics

The four actuated joints of the robot are connected serially and all joint axes intersect at the RCM point as shown in Figure 2. The first rotation about axis RCM0 is described by angle ϕ_0, the second rotation about RCM1 is described by angle ϕ_1, and the third rotation about the probe axis is described by ϕ_2. The translational displacement along the probe axis is described by the variable d.

For convenience, a global frame $\boldsymbol{G}\{x_G, y_G, z_G\}$ is fixed on the RCM point, with z_G aligned with the RCM0 axis. A zero-configuration is defined for the fully collapsed structure of the RCM mechanism (ϕ_1), and the remaining axes are at their midrange location (ϕ_0, ϕ_2, d). Axis x_G is aligned with the RCM1 joint axis and y_G is perpendicular to the plane defined by the RCM0 and RCM1 axes. The end-effector frame $\boldsymbol{EE}\{x_{EE}, y_{EE}, z_{EE}\}$ is placed on the tip of the probe with x_{EE} aligned with the probe axis and y_{EE} parallel to x_G in the zero-configuration. The angle between axis RCM0 and the probe axis is fixed by the design, with an offset $\theta = 60°$.

The forward kinematics to the end effector is derived by first evaluating the orientation of a frame attached to the RCM after rotations about the three axes. Then the position and orientation of the end-effector is found with a d translation along the x_{EE} axis. The overall transformation matrix is:

$$T = T_{\phi_0} T_{\theta,\phi_1} T_{\phi_2} T_d T_{EE} \quad (1)$$

where, the first rotation is ϕ_0, then $\phi_1 - \theta$ and finally ϕ_2, all about the axes of the rotated frames. The described matrices are:

$$T_{\phi_0} = \begin{pmatrix} \cos\phi_0 & \sin\phi_0 & 0 & 0 \\ -\sin\phi_0 & \cos\phi_0 & 0 & 0 \\ 0 & 0 & 0 & 0 \\ 0 & 0 & 0 & 1 \end{pmatrix} \quad (2)$$

$$T_{\theta,\phi_1} = \begin{pmatrix} 1 & 0 & 0 & 0 \\ 0 & \cos(\phi_1 - \theta) & \sin(\phi_1 - \theta) & 0 \\ 0 & -\sin(\phi_1 - \theta) & \cos(\phi_1 - \theta) & 0 \\ 0 & 0 & 0 & 1 \end{pmatrix} \quad (3)$$

$$T_{\phi_2} = \begin{pmatrix} \cos\phi_2 & \sin\phi_2 & 0 & 0 \\ -\sin\phi_2 & \cos\phi_2 & 0 & 0 \\ 0 & 0 & 0 & 0 \\ 0 & 0 & 0 & 1 \end{pmatrix} \quad (4)$$

Next, there is a translation along the probe axis by d:

$$T_d = \begin{pmatrix} 1 & 0 & 0 & 0 \\ 0 & 1 & 0 & 0 \\ 0 & 0 & 1 & -d \\ 0 & 0 & 0 & 1 \end{pmatrix} \quad (5)$$

Finally, the coordinate system is rotated to match the end-effector frame EE:

$$T_{EE} = \begin{pmatrix} 0 & -1 & 0 & 0 \\ 0 & 0 & 1 & 0 \\ -1 & 0 & 1 & 0 \\ 0 & 0 & 0 & 1 \end{pmatrix} \quad (6)$$

The corresponding overall transformation matrix is obtained as follow:

$$T = \begin{pmatrix} T_{1,1} & T_{1,2} & T_{1,3} & T_{1,4} \\ T_{2,1} & T_{2,2} & T_{2,3} & T_{2,4} \\ T_{3,1} & T_{3,2} & T_{3,3} & T_{3,4} \\ T_{4,1} & T_{4,2} & T_{4,3} & T_{4,4} \end{pmatrix} \quad (7)$$

Detailed expressions of each element are given in appendix.

B. Inverse Kinematics

The joint angles for a given position and orientation of the TRUS probe are determined by solving the inverse kinematics problem. The joint angles are determined from the overall transformation matrix (7), as:

$$T_{3,1} = -\cos(\phi_1 - \theta), \quad \phi_1 = \theta - \cos^{-1}(-T_{3,1}) \quad (8)$$

From software and hardware limits, ϕ_1 range is $-20° < \phi_1 < 35°$, with $\theta = 60°$, $-80° < (\phi_1 - \theta) < -25°$, and therefore solution for ϕ_1 is unique. Next, the translation is determined from:

$$T_{3,4} = -d\cos(\phi_1 - \theta) = dT_{3,1}, \quad d = \frac{T_{3,4}}{T_{3,1}} \quad (9)$$

The rotation ϕ_2 is found from:

$$\begin{aligned} T_{3,2} &= -\sin(\phi_1 - \theta)\sin\phi_2 \\ T_{3,3} &= -\sin(\phi_1 - \theta)\cos\phi_2 \\ \phi_2 &= \tan^{-1}\left(\frac{T_{3,2}}{T_{3,3}}\right) \end{aligned} \quad (10)$$

Finally, ϕ_0 is determined from:

$$\begin{aligned} T_{1,1} &= -\sin\phi_0 \sin(\phi_1 - \theta) \\ T_{2,1} &= -\cos\phi_0 \sin(\phi_1 - \theta) \\ \phi_0 &= \tan^{-1}\left(\frac{T_{1,1}}{T_{2,1}}\right) \end{aligned} \quad (11)$$

C. End-effector force measurement

For clinical application, the TRUS Robot presents several safety features such as redundant angular encoders and watchdog circuits, and is equipped with force sensors. Five piezo-resistive force sensors (Kistler SlimLine type 9131 B21) are built in the TRUS driver module.

Figure 3 shows the placement of the sensors. The sensors measure the interaction between the TRUS driver and the probe so that the interaction between the probe and the patient can be estimated.

The force sensors are aligned with the axis of the end-effector coordinate system and all force vectors measured from the sensors intersect with the probe axis (X_{EE}). This arrangement simplifies torque calculations. Two sensors measure forces in the Z_{EE} direction, another two sensors measure in the Y_{EE} direction, and the last one measures in the X_{EE} direction. This placement of the sensors allows measurement of all 3 external forces and 2 torques about Y_{EE} and Z_{EE}. Torque about the probe axis is not measured, since it does not impact the pressure applied by the probe and is unlikely to impact safety.

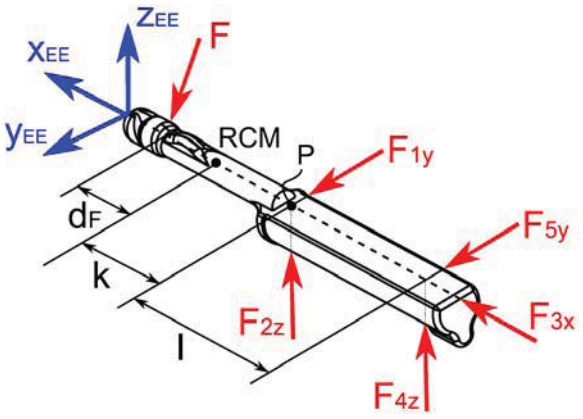

Figure 3: Free body diagram with sensed forces

For static force analysis, the corresponding reaction forces measured on the probe adapter are denoted as F_{ij} with i as the number of the respective force sensor 1~5 and j denoting the force direction. First, assume that a force $F = \{F_x, F_y, F_z\}$ is applied to a probe on a point at distance d_F measured from the RCM point. The distances from the RCM to the sensors are given by k and l, one being constant ($l = 118\,mm$) and the other (k) varying with the translation of the probe ($k = 111 - d$). A point P is defined at the intersection point of F_{1y} and F_{2z}. The force equilibrium equation $\sum F = 0$ is:

$$F_x = F_{3x}, \; F_y = -F_{1y} - F_{5y}, \; F_z = -F_{2z} - F_{4z} \quad (12)$$

The applied moment around point P can be evaluated as

$$M_z = F_{4z}l, \qquad M_y = F_{5y}l \quad (13)$$

and moments equilibrium $\sum M_p = 0$ yields:

$$(d_F + k)F_z - F_{4z}l = 0, \; (d_F + k)F_y - F_{5y}l = 0 \quad (14)$$

Substituting F_z in (13) with (12) yields the location of the equivalent concentrated force $F = \{F_x, F_y, F_z\}$ acting on the probe. The magnitude of the equivalent force and its location describe the interaction between the probe and the patient.

$$d_F = \frac{lF_{4z}}{-(F_{4z} + F_{2z})} - k \quad (15)$$

D. Setup and probe calibration

The TRUS robot, its personal computer (PC) controller, and an ultrasound machine are shown in Figure 4. The robot is attached to a custom sturdy rail attached to the table. A connection and box is mounted at the base of the robot to house force amplifiers, to minimize the length of the force sensor cables. The remaining control electronics are housed in the PC case. Different TRUS probes can be mounted on the TRUS robot with special probe adapters. We are currently

Figure 4: Setup of TRUS Robot

using the Shimadzu UB10R-065U, Hitachi EUP-U533, and Hitachi EUP-V53W probes.

For tracking the position of the ultrasound image, its frame needs to be registered to the robot coordinate system. Part of the transformation from the robot to the case of the probe is known from kinematics, but the location of the images with respect to the case needs to be determined. In this study we assume that the probes are carefully manufactured, so that the image frame is properly aligned with the case. The remaining image scale and origin offset parameters are determined by experimental calibration. This was done individually for each probe by imaging a grid of nylon strings in a water basin, as usual.

E. Software

Robot control software is written in Visual C++ (Microsoft, Redmond, WA) using libraries of the motion control card (MC8000, PMDI, Victoria, B.C). Robot motion can be commanded by either joystick input or numeric software commands. For safety, an independent hardware watchdog circuit monitors the activity of the robot and its control software, automatically disabling the system in case of malfunction.

The software also captures image slices from the ultrasound machine with a frame grabber (Matrox Orion HD, Quebec, Canada). Images are saved in DICOM format. Standard DICOM images from ultrasound do not typically include orientation information, but the DICOM standards include tags to fully describe the location of the image frame. Position information from the robot is saved in the corresponding DICOM tags.

Visualization and further processing of the DICOM images is done with the Amira Visualization software (Visage Imaging, San Diego, CA) with custom modules written in Visual C++. A custom module reads the frame localization tags of each image frame and represents the image in the orientation in which it was acquired.

Oriented 2D image slices that span a volume are then mapped to 3D image voxels. These may be displayed in various modes, such as re-sliced images, volume rendering, or segmented as needed. Volume rendering is an especially promising 3D display mode because it does not require time consuming segmentation. Volume rendering displays each image voxel translucent, and light absorption through the voxel is correlated to its brightness according to a scale factor.

III. RESULTS

A. 3D Imaging:

3D ultrasound imaging was first tested in-vitro using a prostate mockup (CIRS Model 053, Norfolk, Virginia). The TRUS probe was placed in the mockup as shown in Figure 5 and the Hitachi EUP-U533 side-fire probe was rotated about its axis (X_{EE}) to collect images. This Hitachi probe has a very long field of view, sufficiently large to cover the entire prostate without having to advance the probe. As such, a rotary scan about the probe axis was used to sweep the prostate volume. This mode also presents the advantage of minimizing prostate deformations during the scan. Rendered images were consistent in prostate size with the models scanned. An example of the volume rendered prostate image together with a slice from the rotary scan is shown in Figure 5.

B. Clinical Application:

The initial clinical application of the TRUS robot is to provide intraoperative ultrasound-based navigation in Robot-Assisted Laparoscopic Prostatectomy (RALP). A tandem robot approach (T-RALP) with the daVinci surgical robot (Intuitive Surgical, Inc., Sunnyvale, CA) is used [13].

During radical prostatectomy, preservation of the neurovascular bundles (NVBs) is very important for post operative recovery of continence and potency. NVBs are very difficult to visualize with laparoscopic camera during RALP due to peri-prostatic tissues and hemorrhage. Image guidance using TRUS has the potential to improve NVB dissection by visualizing the vessels accompanying the NVB with Doppler ultrasound image.

The TRUS Robot is especially useful for RALP because the setup of the daVinci system leaves no room for a human to handle the probe. The TRUS robot presents a compact design that meets this space constraint without interference with the

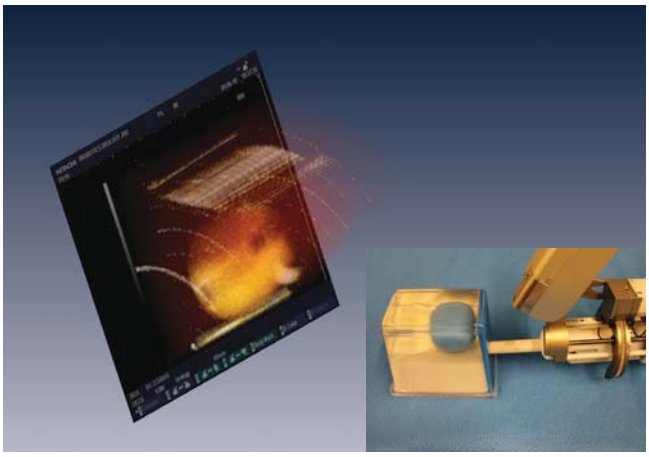

Figure 5: Volume rendering of the prostate mockup

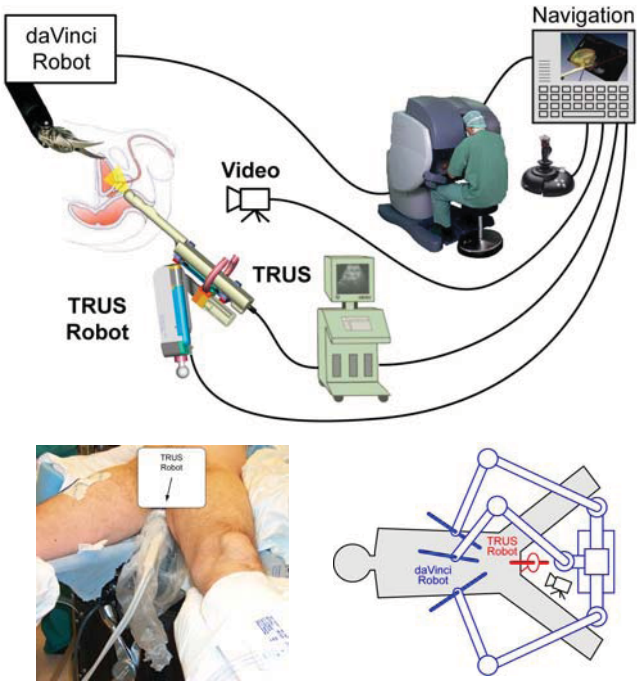

Figure 6 T-RALP setup

patient or the daVinci robot. Figure 6, shows the schematic setup of the T-RALP operation including the patient and the two robots. The TRUS robot is placed between daVinci and the patient. The robot acquires images of the prostate during prostatectomy. These are presented to the surgeon on the daVinci console (using TilePro display).

A clinical study of T-RALP is currently in progress [13] with 37 patients accrued thus far. Figure 7 shows an example of prostate ultrasound and Doppler activity observed in one of the cases. A rotary scan was performed with the TRUS robot. The image shows the tooltip location of one of the daVinci instruments as hyper-echoic marks, momentarily in close proximity of Doppler activity, suggesting proximity to NVB. Post-operative 3D reconstruction of the prostate shows the TRUS probe, one of the image slices of the rotary scan, and the segmented geometry of the prostate, urethra, and possible location of the NVB.

IV. Conclusion and Future Work

A novel TRUS probe manipulator designed for image-guided prostate interventions is presented. The robot provides manipulation of TRUS probe and adds scanning capabilities to conventional 2D ultrasound. Scanning is verified in-vitro and demonstrated clinically. The robot is sufficiently compact to meet space constraints during RALP.

T-RALP results of clinical significance will be derived from the ongoing study. Future studies and applications of the TRUS robot include prostate biopsy. For this, robotic motion will also be instrumental for targeting biopsy locations defined in the image space.

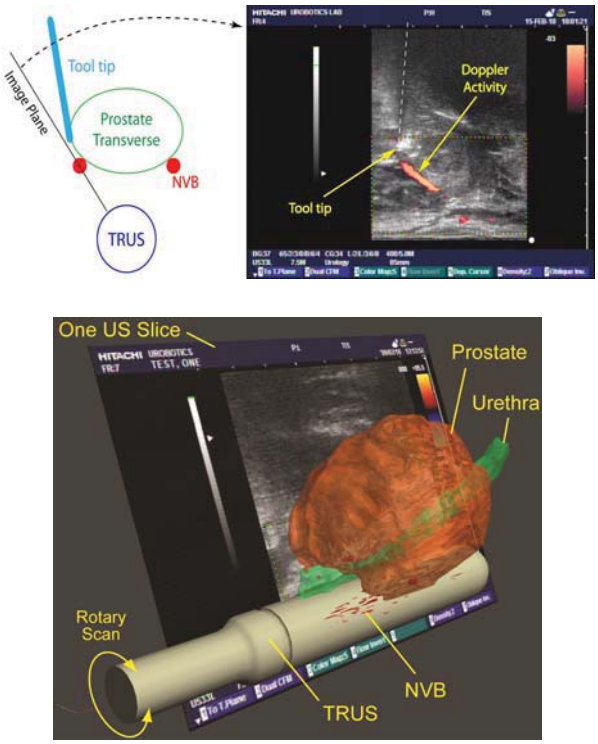

Figure 7: Intra-operative ultrasound image of prostate and adjacent Doppler activity during T-RALP and postoperative 3D reconstruction

Appendix

$$T_{1,1} = -\sin\phi_0 \sin(\phi_1 - \theta)$$
$$T_{1,2} = -\cos\phi_0 \cos\phi_2 + \sin\phi_0 \cos(\phi_1 - \theta)\sin\phi_2$$
$$T_{1,3} = \cos\phi_0 \sin\phi_2 + \sin\phi_0 \cos(\phi_1 - \theta)\cos\phi_2$$
$$T_{1,4} = -d\sin\phi_0 \sin(\phi_1 - \theta)$$

$$T_{2,1} = -\cos\phi_0 \sin(\phi_1 - \theta)$$
$$T_{2,2} = \sin\phi_0 \cos\phi_2 + \cos\phi_0 \cos(\phi_1 - \theta)\sin\phi_2$$
$$T_{2,3} = -\sin\phi_0 \sin\phi_2 + \cos\phi_0 \cos(\phi_1 - \theta)\cos\phi_2$$
$$T_{2,4} = -d\cos\phi_0 \sin(\phi_1 - \theta)$$

$$T_{3,1} = -\cos(\phi_1 - \theta) \qquad T_{3,2} = -\sin(\phi_1 - \theta)\sin\phi_2$$
$$T_{3,3} = -\sin(\phi_1 - \theta)\cos\phi_2 \qquad T_{3,4} = -d\cos(\phi_1 - \theta)$$

$$T_{4,1} = T_{4,2} = T_{4,3} = 0 \quad T_{4,4} = 1$$

References

[1] D. Stoianovici, *et al.*, "AcuBot: A robot for radiological interventions," *Ieee Transactions on Robotics and Automation,* vol. 19, pp. 927-930, Oct 2003.

[2] H. S. S. Ho, *et al.*, "Robotic ultrasound-guided prostate intervention device: system description and results from phantom studies," *International*

Journal of Medical Robotics and Computer Assisted Surgery, vol. 5, pp. 51-58, Mar 2009.

[3] J. Hong*, et al.*, "An ultrasound-driven needle-insertion robot for percutaneous cholecystostomy," *Phys Med Biol,* vol. 49, pp. 441-55, Feb 7 2004.

[4] A. Patriciu*, et al.*, "Automatic brachytherapy seed placement under MRI guidance," *Ieee Transactions on Biomedical Engineering,* vol. 54, pp. 1499-1506, Aug 2007.

[5] E. M. Boctor*, et al.*, "Three-dimensional ultrasound-guided robotic needle placement: an experimental evaluation," *Int J Med Robot,* vol. 4, pp. 180-91, Jun 2008.

[6] B. Maurin*, et al.*, "A Patient-Mounted Robotic Platform for CT-Scan Guided Procedures," *Ieee Transactions on Biomedical Engineering,* vol. 55, pp. 2417-2425, Oct 2008.

[7] N. Zemiti*, et al.*, "LPR: A CT and MR-compatible puncture robot to enhance accuracy and safety of image-guided interventions," *Ieee-Asme Transactions on Mechatronics,* vol. 13, pp. 306-315, Jun 2008.

[8] J. Xu*, et al.*, "Three-dimensional ultrasound image-guided robotic system for accurate microwave coagulation of malignant liver tumours," *Int J Med Robot,* vol. 6, pp. 256-68, Sep 2010.

[9] R. W. Prager*, et al.*, "Stradx: real-time acquisition and visualization of freehand three-dimensional ultrasound," *Med Image Anal,* vol. 3, pp. 129-40, Jun 1999.

[10] P. Abolmaesumi*, et al.*, "Image-guided control of a robot for medical ultrasound," *Ieee Transactions on Robotics and Automation,* vol. 18, pp. 11-23, Feb 2002.

[11] T. K. Podder*, et al.*, "MIRAB: An Image-Guided Multichannel Robot for Prostate Brachytherapy," *International Journal of Radiation Oncology Biology Physics,* vol. 78, pp. S810-S810, 2010.

[12] D. Stoianovici, "Remote center of motion robotic system and method," U.S. Patent 7,021,173, 2006

[13] M. Han*, et al.*, "Tandem-robot assisted laparoscopic radical prostatectomy to improve the neurovascular bundle visualization: a feasibility study," *Urology,* vol. 77, pp. 502-6, Feb 2011.